Passive Intermodulation in Finite Lengths of Printed Microstrip Lines

Dmitry E. Zelenchuk, *Member, IEEE*, Aleksey P. Shitvov, Alexander G. Schuchinsky, *Senior Member, IEEE*, and Vincent F. Fusco, *Fellow, IEEE*

***Abstract*—This paper addresses the theoretical aspects of passive intermodulation (PIM) generation in printed transmission lines. In order to elucidate the mechanisms of PIM generation, a new model of the transmission line length with distributed nonlinearity is proposed. The developed model has been validated by the near-field measurements of PIM product distributions along the microstrip lines. The contributions of nonlinear mixing, power dissipation, and load matching to PIM products have been analyzed in detail. The obtained results reveal the fundamental properties of PIM generation in finite lengths of printed lines with distributed nonlinearity and identify possible means for PIM mitigation. It was shown for the first time that the reverse PIM products in a matched transmission line with distributed nonlinearity are generated due to nonlinear scattering.**

***Index Terms*—Distributed nonlinearity, intermodulation distortion, passive intermodulation (PIM), printed circuits.**

I. Introduction

PASSIVE intermodulation (PIM) is known for its detrimental effect on performance of telecommunication systems. It manifests itself as spurious signals in receiver or transmitter frequency bands. First discovered as a product of nonlinear mixing on rusty metallic contacts [1], [2], PIM phenomena were further observed in ferrite circulators [3], waveguide and cable joints [4], duplexers [5], attenuators [6], and antennas [7]. PIM sources in these devices have been extensively studied, and the progress in understanding the underlying physical mechanisms has led to the development of the means for PIM mitigation [1], [4]–[6], [8]–[10].

Recent trends in microwave technology have brought forward printed circuit boards (PCBs) as an attractive platform for planar and integrated RF front end. However, despite the high performance and low cost, the wide use of printed components in power devices is hindered by the experimental observations that PCB laminate itself can generate PIM products. Therefore, identification and understanding of PIM generation mechanisms are vital for successful application of PCBs in high-performance printed antennas, feeders, multiplexers, circuits, interconnects, backpanels, etc.

The topic of PIM generation on printed lines is scarcely explored, and only a few studies have addressed it to date. Several potential factors contributing to PIM generation have been suggested in [11]–[15]. However, the underlying mechanisms of PIM generation still remain unclear. The lack of reliable theoretical models of PIM generation in printed transmission lines also restrains design of low PIM devices.

The network models based on localized nonlinearity approach were proposed in [16]–[18]. While being appropriate for analysis of lumped nonlinearities, created by point defects such as imperfect soldered joints, these models fail to explain certain experimental observations. For example, the fact that, in a matched line, the PIM level measured at the output port (forward PIM) is higher than that measured at the input port (reverse PIM) has no explanation in the localized nonlinearity model.

Since PIM products on printed lines are usually more than 100 dB below the carrier power level, it is reasonable to characterize PIM sources as a weak distributed nonlinearity of the transmission line. This assumption is supported by the experimental observations of PIM products on microstrip traces, which indicate that the copper foil structure, surface roughness, finishing of the etched traces, and foil–dielectric interfaces are the major contributors to PIM generation (cf. [11], [14], and [15]). The randomly distributed microscopic nonlinearities inherent to these constitutive elements of PCB laminate act as PIM sources closely associated with the current flow on the printed traces. Based on these observations, the authors proposed the theoretical model of PIM generation on printed lines and the initial results of PIM modeling, reported in [19] and [20], proved its validity.

In this paper, the theory of distributed PIM production on weakly resistively nonlinear transmission lines of finite lengths with arbitrary termination and source impedances is presented and applied to comprehensive study of PIM generation in printed lines. The developed model is further validated here by near-field probing of PIM product distributions on printed microstrip lines using the setup of [21] and [22]. Impact of various factors on PIM generation is modeled and analyzed in detail, and a means for PIM mitigation is suggested.

This paper is organized as follows. The model and solution of the corresponding mathematical problem for the distributed PIM product generation on nonlinear transmission lines are described in Section II. The model validation is presented in Section III. The asymptotic solution for the perfectly matched

Manuscript received May 15, 2008; revised July 30, 2008. First published October 24, 2008; current version published November 07, 2008. This work was supported by the Engineering and Physical Sciences Research Council (U.K.) under EPSRC Grant EP/C00065X/1.

The authors are with the Institute for Electronics, Communications and Information Technologies (ECIT), Queen's University of Belfast, BT3 9DT Belfast, U.K. (e-mail: d.zelenchuk@qub.ac.uk; a.shitvov@qub.ac.uk; a.schuchinsky@qub.ac.uk; v.fusco@ecit.qub.ac.uk).

Color versions of one or more of the figures in this paper are available at http://ieeexplore.ieee.org.

Digital Object Identifier 10.1109/TMTT.2008.2005886

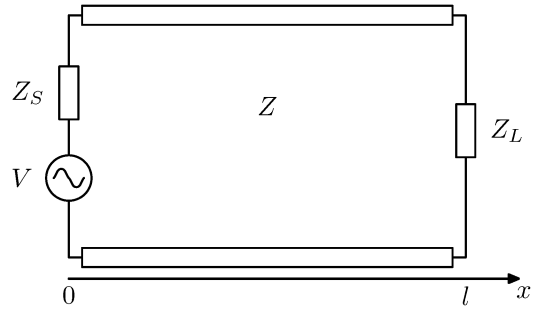

Fig. 1. Section of a nonlinear transmission line.

line is discussed in Section IV in order to illustrate the fundamental properties of PIM generation, and in particular, the effect of insertion loss. In Section V, the mechanisms of PIM generation in finite segments of mismatched lines, including the effects of the load reflection and line length, are discussed in detail.

II. Theory

The main concepts of the model, introduced in [19], are elaborated in this section to provide a generic framework for the comprehensive analysis of distributed PIM generation on the printed lines of finite length. It will be shown that the account of the line length is crucial for self-consistent description of PIM phenomena on printed lines.

A. General Approach

Let us consider a section of transmission line with distributed weakly nonlinear resistance, as shown in Fig. 1. The line is excited by the two-tone generator with voltage V and internal impedance Z_S, and terminated in the load Z_L. The terminations are assumed to be linear.

Electromagnetic wave propagation in a transmission line with the distributed weakly nonlinear resistance is governed by the telegrapher's equations for voltage $U(x,t)$ and current $I(x,t)$ [23]

$$\frac{\partial I(x,t)}{\partial x} = -\left(C\frac{\partial U(x,t)}{\partial t} + GU(x,t)\right) \tag{1}$$

$$\frac{\partial U(x,t)}{\partial x} = -\left(L\frac{\partial I(x,t)}{\partial t} + R(I)I(x,t)\right) \tag{2}$$

where L, C, $R(I)$, and G are per-unit-length parameters of the transmission line.

The weakly nonlinear resistance $R(I)$ is assumed to be current dependent and can be approximated by a polynomial. Although the system of (1) and (2) can be solved for the polynomial of any order, we restrict the analysis to the third-order nonlinearity, and discuss the main features of the third-order PIM (PIM3) production only. The higher order nonlinear terms usually cause much weaker response [24], and therefore, are not considered in this paper. In this case, the nonlinear resistance can be represented in the form

$$R(I) = R_0 + R_2 I^2 \quad R_0 \gg R_2 I^2. \tag{3}$$

where R_0 is linear resistance and R_2 is the nonlinearity coefficient.

Substituting (3) into (2) and combining the result with (1), we obtain a nonlinear differential equation for $I(x,t)$ as follows:

$$\frac{\partial^2 I(x,t)}{\partial x^2} - CL\frac{\partial^2 I(x,t)}{\partial t^2} - (CR_0+GL)\frac{\partial I(x,t)}{\partial t} - GR_0 I(x,t) = R_2 I^2(x,t)\left(3C\frac{\partial I(x,t)}{\partial t} + GI(x,t)\right). \tag{4}$$

The steady-state solution for PIM products in a weakly nonlinear line can be obtained by the perturbation method combined with Fourier-series expansion [24]. Now $I(x,t)$ is sought in the form

$$I(x,t) = \sum_{k=0}^{\infty}\sum_{q=-\infty}^{\infty}\sum_{p=-\infty}^{\infty} R_2^k \tilde{I}_{q,p,k}(x)\exp(i\omega_{q,p}t) \tag{5}$$

where $\omega_{q,p} = q\omega_1 + p\omega_2$; ω_1 and ω_2 are angular frequencies of the carrier tones and $\sum_{k=0}^{\infty} R_2^k \tilde{I}_{q,p,k}(x)$ is the current distribution of the frequency harmonic $\omega_{q,p}$.

Substituting (5) in (4) and collecting the terms with the same frequencies and powers k of R_2, one obtains the system of linear inhomogeneous differential equations for $\tilde{I}_{q,p,k}(x)$

$$\left(\frac{d^2}{dx^2} - \gamma_{q,p}^2\right)\tilde{I}_{q,p,k}(x) = \sum_{v=0}^{k-1}\sum_{j=0}^{v}\sum_{m=-\infty}^{\infty}\sum_{n=-\infty}^{\infty}\sum_{r=-\infty}^{\infty}\sum_{s=-\infty}^{\infty}(3i\omega_{q-r,p-s}C+G) \times \tilde{I}_{m,n,j}(x)\tilde{I}_{r-m,s-n,v-j}(x)\tilde{I}_{q-r,p-s,k-v-1}(x). \tag{6}$$

where $\gamma_{q,p} = \sqrt{(R_0 + i\omega_{q,p}L)(G + i\omega_{q,p}C)} \approx i\beta_{q,p} + \alpha$ is the complex wavenumber, and for the sake of brevity, function $\tilde{I}_{q,p,k}(x)$ will be referred to as the current distribution.

It is necessary to emphasize that the number of harmonics contributing to the kth term in the series (5) is restricted by the perturbation order k. Indeed, in accordance with (6), only the harmonics with the indices satisfying the following condition are required for evaluating $\tilde{I}_{q,p,k}(x)$:

$$|q| + |p| = 2d + 1, \qquad d \in [0,k]. \tag{7}$$

Thus, the system of (6) can be solved successively for each k independently. At $k = 0$, (6) becomes the homogeneous equation, and its solution has the form

$$\tilde{I}_{q,p,0}(x) = A_{q,p,0}\exp(-\gamma_{q,p}x) + B_{q,p,0}\exp\left(-\gamma_{q,p}(l-x)\right). \tag{8}$$

Hence, $\tilde{I}_{q,p,0}(x)$ represents a linear wave of the current on the transmission line at individual frequency harmonic.

At $k = 1$, (6) becomes the inhomogeneous wave equation, and its right-hand side contains only the known functions $\tilde{I}_{q,p,0}(x)$ obtained for $k = 0$ at the previous step. The function $\tilde{I}_{q,p,1}(x)$ is of particular interest in this study because it describes the current distribution of PIM3 products. The solution of (6) at $k = 1$ can be represented in the following form:

$$\tilde{I}_{q,p,1}(x) = A_{q,p,1}\exp(-\gamma_{q,p}x) + B_{q,p,1}\exp\left(-\gamma_{q,p}(l-x)\right) + F_{q,p,1}(x) \tag{9}$$

where $F_{q,p,1}(x)$ is a particular solution of the inhomogeneous differential equation (6). The function $F_{q,p,1}(x)$ is unique for each frequency, and its closed-form expression is presented in the Appendix for PIM3 frequency $\omega_{2,-1}$, which is used for evaluating PIM3 products throughout this paper.

Due to space limitations, only the results for PIM3 are discussed in this paper. However, higher order PIM products can be readily retrieved at $k > 1$ with the aid of (6), (8), and (9) treated in a similar fashion as for $k = 1$.

B. Boundary Conditions

The solutions of (6) obtained in Section II-A for $k = 0, 1$ describe only the eigenwaves on the transmission line, but their magnitudes still remain undefined. Indeed, the expressions for the current distributions (8) and (9) contain unknown coefficients, which are determined by the respective boundary conditions at the line terminals. Taking into account the relationship (1) between the current $\tilde{I}_{q,p,k}(x)$ and voltage $\tilde{U}_{q,p,k}(x)$ distributions on the line, we obtain for each harmonic in (5)

$$\tilde{U}_{q,p,k}(x) = \frac{1}{i\omega_{q,p}C + G}\frac{d\tilde{I}_{q,p,k}(x)}{dx}.$$

Thus, the boundary conditions at $x = 0$ and $x = l$ have the following form:

$$\begin{aligned} Z_S(\omega_{q,p})\tilde{I}_{q,p,k}(0) - \frac{\tilde{V}_{q,p}}{R_2^k}\delta_{0,k} &= \frac{1}{i\omega_{q,p}C + G}\left.\frac{d\tilde{I}_{q,p,k}(x)}{dx}\right|_{x=0} \\ -Z_L(\omega_{q,p})\tilde{I}_{q,p,k}(l) &= \frac{1}{i\omega_{q,p}C + G}\left.\frac{d\tilde{I}_{q,p,k}(x)}{dx}\right|_{x=l} \end{aligned} \tag{10}$$

where $Z_S(\omega_{q,p})$ and $Z_L(\omega_{q,p})$ are the impedances of the source and load, $\tilde{V}_{q,p}$ is the complex Fourier amplitude of the source signal at frequency $\omega_{q,p}$, and $\delta_{0,k}$ is the Kronecker delta [25].

It is necessary to emphasize that the use of the boundary conditions (10) is essential to obtain the physically meaningful solution of the PIM problem. In particular, proper consideration of the boundary conditions at the line terminals has enabled us to explain the experimental observations of the reverse PIM generation on matched lines. Earlier, this phenomenon either could not be modeled [24] or was attributed to the carrier reflection from the load only [26].

Since the termination loads are assumed here to be linear, the boundary conditions can be applied successively to each perturbation order. First, one obtains the coefficients in the current distributions $\tilde{I}_{q,p,0}(x)$ [cf. (8)]

$$\begin{aligned} A_{q,p,0} &= \frac{\tilde{V}_{q,p}}{D_{q,p}\left(Z_S(\omega_{q,p}) + Z_0(\omega_{q,p})\right)} \\ B_{q,p,0} &= -\frac{\tilde{V}_{q,p}\Gamma_L(\omega_{q,p})u_{q,p}}{D_{q,p}\left(Z_S(\omega_{q,p}) + Z_0(\omega_{q,p})\right)} \end{aligned} \tag{11}$$

where $D_{q,p} = 1 - \Gamma_L(\omega_{q,p})\Gamma_S(\omega_{q,p})u_{q,p}^2$, $u_{q,p} = \exp(-\gamma_{q,p}l)$, $\Gamma_L(\omega_{q,p})$, and $\Gamma_S(\omega_{q,p})$ are the load and source reflection coefficients [23]; q and p satisfy (7) at $k = 0$; and $Z_0(\omega_{q,p}) = \sqrt{(R_0 + i\omega_{q,p}L)/(G + i\omega_{q,p}C)}$ is the characteristic impedance of the transmission line, which is readily available for many types of the canonical transmission lines, including microstrip lines (see, e.g., [27]).

The function $F_{q,p,1}(x)$ can then be evaluated and unknown amplitudes for the first order of perturbation with q and p satisfying (7) at $k = 1$ can be determined from the boundary conditions (10)

$$\begin{aligned} A_{q,p,1} &= \frac{1}{D_{q,p}}\left(\frac{S_{q,p}}{Z_S(\omega_{q,p}) + Z_0(\omega_{q,p})} - \frac{u_{q,p}Q_{q,p}\Gamma_S(\omega_{q,p})}{Z_L(\omega_{q,p}) + Z_0(\omega_{q,p})}\right) \\ B_{q,p,1} &= \frac{1}{D_{q,p}}\left(\frac{Q_{q,p}}{Z_L(\omega_{q,p}) + Z_0(\omega_{q,p})} - \frac{u_{q,p}S_{q,p}\Gamma_L(\omega_{q,p})}{Z_S(\omega_{q,p}) + Z_0(\omega_{q,p})}\right) \end{aligned}$$

where

$$\begin{aligned} S_{q,p} &= Z_0(\omega_{q,p})\Psi_{q,p,1}(0) - Z_S(\omega_{q,p})F_{q,p,1}(0) \\ Q_{q,p} &= -\left(Z_0(\omega_{q,p})\Psi_{q,p,1}(l) + Z_L(\omega_{q,p})F_{q,p,1}(l)\right) \\ \Psi_{q,p,1}(x) &= \frac{1}{\gamma_{q,p}}\frac{dF_{q,p,1}(x)}{dx}. \end{aligned}$$

The expressions derived above describe the complete self-consistent solution of (1) and (2) up to the first perturbation order, which is sufficient to evaluate the PIM3 response. For further quantitative investigation, power of the reverse P_{rev} and forward P_{forw} PIM3 products are defined at frequency $\omega_{2,-1}$ as follows:

$$\begin{aligned} P_{\text{rev}} &= R_2^2\frac{1}{2}\text{Re}\left\{\tilde{I}_{2,-1,1}(0)\tilde{U}_{2,-1,1}(0)^*\right\} \\ P_{\text{forw}} &= R_2^2\frac{1}{2}\text{Re}\left\{\tilde{I}_{2,-1,1}(l)\tilde{U}_{2,-1,1}(l)^*\right\} \end{aligned} \tag{12}$$

where $*$ and Re stand for complex conjugate and real part of complex quantities, respectively.

III. Experimental Validation

For the purpose of validation of the developed theoretical model, simulation results have been compared with near-field measurements of PIM3 products on microstrip lines.

The measurements were performed using the Summitek Instruments PIM analyzer SI-900B. A 50-Ω microstrip line of the length 914 mm was fabricated on 0.76-mm-thick substrate with permittivity $\varepsilon_r = 3$ and $\tan\delta = 0.0026$. The line terminated in the low-PIM matched load was fed by two 44-dBm carriers at frequencies $f_1 = 935$ MHz and $f_2 = 960$ MHz. The near field at PIM3 frequency was sampled with a capacitive probe made of the coaxial cable connected to the input port of the PIM analyzer. The probe was oriented horizontally and then vertically providing average coupling of -39.6 and -33.1 dB, respectively, to the test line [22]. Such weak coupling ensured negligible probe influence on the PIM generation in the line. The actual PIM3 power rate $P_V(x)$ has been evaluated as the difference in decibels between the measured PIM $P_{\text{meas}}(x)$ and the probe coupling $P_{\text{coupl}}(x)$ at frequency $2f_1 - f_2 = 910$ MHz (cf. [21])

$$P_V(x) = P_{\text{meas}}(x) - P_{\text{coupl}}(x). \tag{13}$$

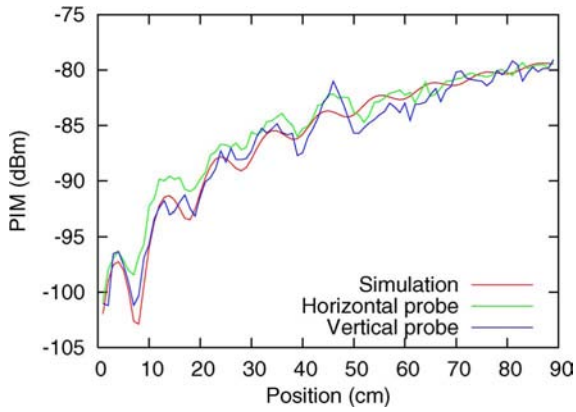

Fig. 2. Comparison of the simulation and near-field PIM3 probing from [22].

The measurement results retrieved with the aid of (13) are displayed in Fig. 2 along with the simulated PIM3 power, defined as

$$P_V(x) = R_2^2 \frac{\left|\tilde{U}_{2,-1,1}(x)\right|^2}{2Z_0(\omega_{2,-1})}. \tag{14}$$

Note that the latter definition of $P_V(x)$ is intrinsically consistent with the near-field measurements, where the capacitive probe picks up the electric field distribution along the microstrip line.

The value of nonlinear parameter $R_2 = 2.6 \times 10^{-4}$ $\Omega\mathrm{A}^{-2}$ m^{-1} has been fitted to equalize the power levels in the simulations and measurements. Ripples on the curves are associated with interference of PIM products traveling in forward and reverse directions, and their magnitudes are affected by matching of the source and load impedances. The effect of reflection at microstrip-to-coaxial transitions was taken into account in the simulation by setting the port impedances to $(49.3 + 2.5i)$ Ω. An excellent agreement with the measurements was achieved when using both horizontal and vertical probes.

The impedance value was fitted to the data. Unfortunately, this parameter is not measurable directly because the reference planes in the model and measurements (including S-parameters) are offset. The values of $|S11|$ measured at the reference planes of the connectors differ only for approximately 5% from the fitted value used at the line ends of the model (soldering points of the connectors in experiments). We believe that such discrepancy is well within uncertainty of our measurement setup and is reasonable for the model used.

Thus, the presented comparison of the simulation and measurement results has fully justified the developed theoretical model and its fitness for the study of the mechanisms of PIM generation on the printed lines.

IV. PIM Generation on Matched Line

A. PIM3 Current Distribution

The closed-form solution obtained above enables modeling of PIM products generated in a length of the line with distributed nonlinearity for various terminations. While the general solution is rather cumbersome, it admits simplifications in several important cases.

The line with perfectly matched source and load terminations at $\omega_{q,p}$ is of particular interest. In this case,

$$\begin{aligned} Z_0(\omega_{q,p}) &= Z_L(\omega_{q,p}) = Z_S(\omega_{q,p}) \\ \Gamma_L(\omega_{q,p}) &= \Gamma_s(\omega_{q,p}) = 0. \end{aligned} \tag{15}$$

When applying the conditions (15) to (9), (11), and (A1), one can obtain a simple expression for the PIM3 current distribution along the line

$$\begin{aligned} \tilde{I}_{2,-1,1}(x) = &-\xi(1+\nu)\exp(-\gamma_{2,-1}x) \\ &+ \xi\exp\left(-(2\gamma_{1,0}+\gamma_{0,-1})x\right) \\ &+ \xi\nu\exp\left(-\gamma_{2,-1}(2l-x)-2\alpha l\right) \end{aligned} \tag{16}$$

where

$$\nu = \frac{\alpha}{\gamma_{2,-1}}$$

$$\xi = \frac{3\tilde{V}_{1,0}^2\tilde{V}_{0,-1}}{32\nu Z_0(\omega_{1,0})^2 Z_0(\omega_{0,-1})Z_0(\omega_{2,-1})(i\beta_{2,-1}+2\alpha)}.$$

Despite no reflection is present in the line, the total current (16) comprises the waves traveling in both forward and reverse directions at PIM3 frequency. Superposition of these waves gives rise to the forward and reverse PIM products at the input and output terminals correspondingly.

Indeed, from (16), the reverse PIM3 current reads

$$\tilde{I}_{2,-1,1}(0) = -\xi\nu\left\{1-\exp(-2i\beta_{2,-1}l-4\alpha l)\right\} \tag{17}$$

and the forward PIM3 current is

$$\tilde{I}_{2,-1,1}(l) = \xi(1+\nu)\exp(-i\beta_{2,-1}l-\alpha l)\left\{\exp(-2\alpha l)-1\right\}. \tag{18}$$

The literature available to date attributes the existence of the reverse PIM products solely to the scattering from the lumped nonlinearity [16]. Otherwise, PIM products would not be even anticipated, e.g., in the analysis of harmonic generation by the semi-infinite nonlinear transmission line [24], where the reverse waves were excluded at the stage of the boundary condition fulfilment. An attempt to address this issue for the line with distributed nonlinearity was made in [26]. However, the approximate model linked the reverse PIM products to the load reflection and no reverse PIM was found in the matched line. Thus, (17) above demonstrates for the first time the mechanism of reverse PIM generation due to nonlinear scattering in a matched transmission line with distributed nonlinearity.

Further analysis of (17) and (18) allows us to explore the effects of the line length, losses, and frequency variations on the PIM3 generation, as well as the means for its mitigation.

B. PIM3 Generation in Lossless Lines

In order to elucidate the mechanisms of PIM3 generation in the low-loss transmission lines, let us consider a lossless line

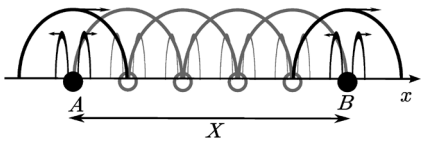

Fig. 3. Traveling wave four-wave mixing. Large semicircles represent carriers' waves, and the small ones correspond to the scattered PIM products.

($\alpha = 0$) first. The reverse PIM3 current distribution (17) then oscillates with magnitude $\xi\nu$ and has nulls at the line lengths

$$l_n = \frac{n\lambda}{2}, \qquad n = 1, 2, \ldots. \tag{19}$$

It is interesting to note that a similar effect of reverse PIM suppression was observed in [16] for the PIM products generated by two point nonlinearities offset from each other for the same distance l_n. In this case, appearance of the nulls was attributed to *linear* interference of the PIM products generated by a pair of nonlinearities. It is necessary to emphasize that although the relationship (19) has the same form as for the pair of lumped nonlinearities, it originates from a fundamentally different mechanism of PIM generation by the distributed nonlinearity. The existence of nulls in the reverse PIM3 distribution is of the practical significance as a means for mitigation of reverse PIM3 by using an appropriate line length in antenna elements, feeders, printed circuits, interconnects, etc.

To evaluate the current of the forward PIM3 products, it is necessary to find the limit of (18) at $\alpha = 0$

$$\lim_{\alpha\to 0} \tilde{I}_{2,-1,1}(l) = -\frac{3l\tilde{V}_{1,0}^2\tilde{V}_{0,-1}\exp(-i\beta_{2,-1}l)}{16Z_0(\omega_{1,0})^2 Z_0(\omega_{0,-1})Z_0(\omega_{2,-1})}. \tag{20}$$

According to (20), the magnitude of the forward PIM3 products linearly grows with the line length in a lossless transmission line. Such growth of forward PIM3 level has a simple physical explanation that in the absence of loss nonlinear conversion of the carriers into PIM harmonics is unrestricted. Such processes are well known in nonlinear optics and a similar mechanism of the second harmonic generation was described in [28].

Alternatively, the mechanisms of the forward and reverse PIM3 generation can be understood in terms of the phase matching in a four-wave mixing process. Let us consider the distributed nonlinearity of the transmission line as a set of discrete infinitely small weakly nonlinear scatterers. In the perfectly matched line, one can admit that the fundamental carriers experience no reflection and travel in the forward direction only. However, the nonlinear conversion occurs at each scatterer, which generates PIM products in both forward and reverse directions [21].

Let us consider PIM3 products generated by a pair of scatterers located at arbitrary positions $x = A$ and $x = B$ in the matched lossless dispersionless nonlinear transmission line (Fig. 3). Assuming that the reference plane is located at $x = A$, PIM3 products generated in both directions at A and B by the carriers of frequencies f_1 and f_2 have the phases $\varphi_A = 0$ and $\varphi_B(X) = (2\beta_{1,0} + \beta_{0,-1})X$, where X is the distance between A and B. On the other hand, the PIM3 products traveling from A to B accrue the phase $\varphi_{AB}(X) = \beta_{2,-1}X$.

Therefore, at any $x = B$, the phase difference between the PIM products generated in forward direction at B and A equals $\Delta_f(X) = \varphi_B(X) - \varphi_{AB}(X)$. Since in the dispersionless line $\beta_{2,-1} = 2\beta_{1,0} + \beta_{0,-1}$, then $\Delta_f(X) = 0$ for any X. Hence, the PIM3 products generated in the forward direction by any pair of scatterers in the line interfere constructively. This results in accruing forward propagating PIM3 products and causes linear growth of the forward PIM3 level with the line length [cf. (20)].

The PIM3 products generated in the reverse direction by the scatterers at $x = A$ and $x = B$ always have a nonzero phase difference $\Delta_r(X) = \varphi_{AB}(X) + \varphi_B(X)$ at any $x = A$. Therefore, whenever $\Delta_r(X)$ equals odd multiples of π, they interfere destructively. The corresponding shortest distance $X_c = \lambda_{2,-1}/4$ is called the coherence distance, where $\lambda_{2,-1}$ is the PIM3 product wavelength. In the line of length X_c, only contributions of the end scatterers are cancelled and the reverse PIM3 level reaches the maximum because responses of the interim scatterers add up. When the line length equals $2X_c$, it contains a full set of the scatterer pairs that PIM3 products cancel each other. This results in annihilation of the reverse PIM products at the line input. Thus, in the matched lossless dispersionless nonlinear transmission line, only the length shorter than $2X_c$ contributes to the reverse PIM3 response, while the line extension for any multiple of $2X_c$ does not change the reverse PIM3 level. This qualitative description of the mechanisms of PIM3 generation is fully consistent with the current distributions (19) and (20) predicted by the model developed in Section II.

C. Effect of Loss on PIM3 Generation

The analysis presented in Section IV-B provides an invaluable insight into the mechanisms of PIM generation in the ideal transmission line, but it is still incomplete without taking into account the effect of damping.

From the physical standpoint, the harmonic generation and dissipation are two competitive processes. In order to estimate the effect of loss on PIM3 products, it is necessary to determine a dependence of the amplitude coefficients in (17) and (18) on the attenuation constant α. From (16), we obtain

$$\xi(\alpha) \propto \frac{1}{\alpha} \quad \nu(\alpha) \propto \alpha \quad \xi(\alpha)\nu(\alpha) = \text{const}. \tag{21}$$

Taking into account (21), one can easily conclude that, in the case of high losses, forward PIM3 products will decay with the line length due to the exponential term in (18). The reverse PIM3 products, in their turn, do not vanish, but rapidly approach the asymptotic level of $-\xi\nu$. To illustrate this effect, the forward and reverse PIM3 products are plotted in Fig. 4 versus the line length for the perfectly matched microstrip line with the parameters specified in Section III.

Due to the competing effects of loss and harmonic generation, magnitude of the forward PIM3 products reaches a maximum at the line length l_f, which is found from (18) as

$$l_f = \frac{\ln 3}{2\alpha}. \tag{22}$$

As shown in Fig. 4, the forward PIM3 products fall below the reverse PIM3 level on longer lines. The line length l_i, at which

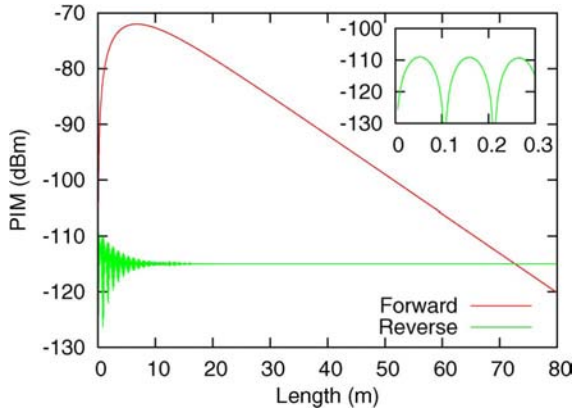

Fig. 4. Simulated PIM3 products on perfectly matched transmission lines (inset displays magnified view of the reverse PIM3 distribution).

the two curves intersect each other, can be obtained from (17) and (18) as

$$l_i \approx \frac{\ln |\nu|^{-1}}{\alpha}. \tag{23}$$

The presented asymptotic estimates of the PIM3 products demonstrate strong correlation between insertion loss (attenuation constant α) and PIM3 production/extinction rate. Higher attenuation causes a decrease of the l_f [cf. (22)], and faster growth of the forward PIM3 level before the maximum is reached and slower decay after that.

D. Frequency Dependence of PIM3 Products

In practice, the PIM harmonics are of particular concern when their frequencies fall close to the carrier tones. Therefore, within the narrow operating bands, the propagation and attenuation constants, and wave impedances of the traveling waves, can be assumed dispersionless. Taking into account that the PIM3 products propagating on printed lines have $\beta_{2,-1} \gg \alpha$, one can then obtain from (16) that

$$\xi(\beta_{2,-1}) = \text{const} \quad \nu(\beta_{2,-1}) \propto \frac{1}{\beta_{2,-1}}. \tag{24}$$

Substitution of (24) into (17) and (18) shows that the reverse PIM3 current is reciprocal of $\beta_{2,-1}$, while the forward PIM3 current is independent of $\beta_{2,-1}$. Since $\beta_{2,-1}$ is proportional to frequency, the reverse PIM3 products should decrease with frequency, while the forward PIM3 level would remain unchanged. However, further taking into account that losses in dielectrics and conductors increase with frequency, one can infer from (17) and (18) that both reverse and forward PIM3 products attenuate at higher frequencies.

It is necessary to note that the frequency dependence of the nonlinear parameter R_2 is *a priori* unknown, and can be affected by the variety of nonlinear processes involved in the PIM generation [8]. Nevertheless, in the narrow frequency band, the frequency dependence of R_2 can be retrieved from the PIM measurements using the qualitative considerations outlined above. For instance, if the reverse PIM3 level increases with frequency, as observed in [29], then the asymptotic behavior of R_2 can be deduced from (12), (17), and (24) as follows:

$$R_2 \propto \beta_{2,-1}^{1+a}, \qquad a > 0. \tag{25}$$

where the parameter a in (25) is determined by the frequency dependences of both nonlinearity and losses.

V. PIM on Mismatched Lines

A. Effect of the Load Reflection on PIM Generation

Since the perfect matching cannot be attained in practice, the condition (15) is satisfied only approximately. Therefore, the total PIM3 current expressed by (9) and (A1) should contain all eight terms that complicates further analytical study. Consequently, the analysis of PIM generation on mismatched lines presented here is based on the numerical simulations performed with the aid of the complete model described in Section II. For the sake of brevity, we consider here only the case of the matched source impedance assuming that the major effect of the source mismatch is limited to the decrease of the carrier power injected in the line (cf. [20]).

The load matching, as observed in [12] and [18], has a strong impact on PIM generation on microstrip lines by lumped sources. Therefore, similar phenomenon has been anticipated for the case of the line with distributed nonlinearity.

In order to illustrate the effect of the load mismatch, we have simulated PIM3 products on a 1-m-long microstrip line with parameters of the experimental specimens described in Section III. Since the simulations were performed in the narrow frequency band, $\Gamma_L(\omega_{2,-1})$ was assumed constant at all frequencies of interest.

Reverse and forward PIM3 products calculated for the entire range of magnitudes and phases of the load reflection coefficient $\Gamma_L(\omega_{2,-1})$ are shown in Figs. 5 and 6. It is demonstrated in Fig. 5 that the reverse PIM3 magnitude monotonically grows with $|\Gamma_L(\omega_{2,-1})|$, and the difference between the extreme cases of the zero and total reflection reaches 30–40 dB. Apparently, this is the result of variation in magnitudes of the standing waves of the carriers and the respective PIM3 products propagating in the reverse direction, as defined in (9), (11), and (A1). A considerable increase of the PIM3 level occurs at the low magnitude of $|\Gamma_L(\omega_{2,-1})| < 0.3$, while at higher values of $|\Gamma_L(\omega_{2,-1})|$, the PIM3 level grows nearly linearly. It is also interesting to note that the phase of $\Gamma_L(\omega_{2,-1})$ has a much weaker effect than its magnitude on the PIM3 generation, and it is discernible only at low $|\Gamma_L(\omega_{2,-1})|$.

Forward PIM3 products exhibit rather different behavior, as illustrated in Fig. 6. The range of $|\Gamma_L(\omega_{2,-1})|$ variation was limited to $|\Gamma_L(\omega_{2,-1})| < 0.9$ because, at higher $|\Gamma_L(\omega_{2,-1})|$, the forward PIM3 magnitude rapidly falls out of the plot scale. In the range of $|\Gamma_L(\omega_{2,-1})|$, shown in Fig. 6, which is of practical importance, the forward PIM3 level varies within 4 dB, which is much less than the reverse one. In addition, it has a maximum—the crest of the surface in Fig. 6. Appearance of this maximum is counterintuitive at first glance because the PIM3 power delivered to the load for certain values of $|\Gamma_L(\omega_{2,-1})|$ appears to be higher than in the case of zero reflection. However,

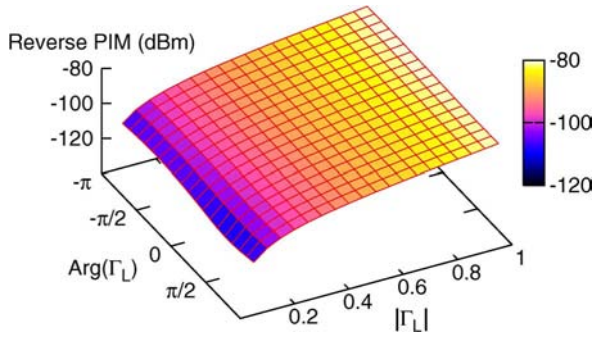

Fig. 5. Reverse PIM3 magnitude on the 1-m-long microstrip line with distributed nonlinearity terminated in the load with reflection coefficient Γ_L.

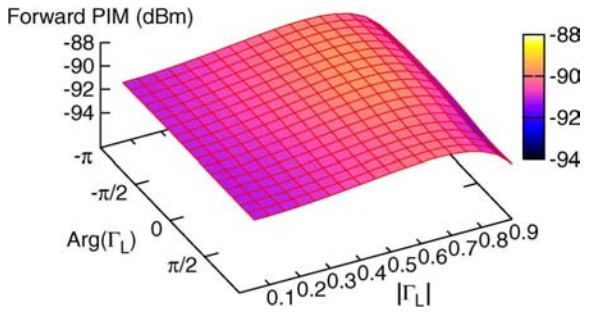

Fig. 6. Forward PIM3 magnitude on the 1-m-long microstrip line with distributed nonlinearity terminated in the load with reflection coefficient Γ_L.

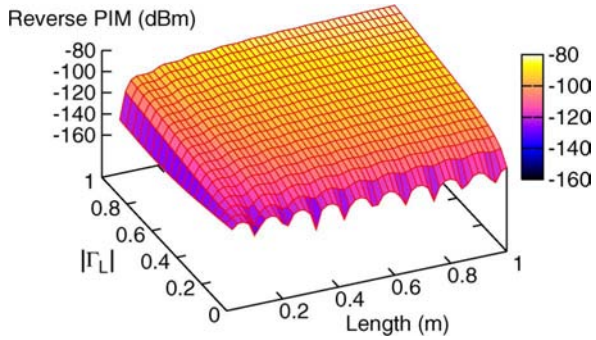

Fig. 7. Reverse PIM3 on the microstrip lines with distributed nonlinearity terminated in the load with reflection coefficient $|\Gamma_L|$ at variable line length.

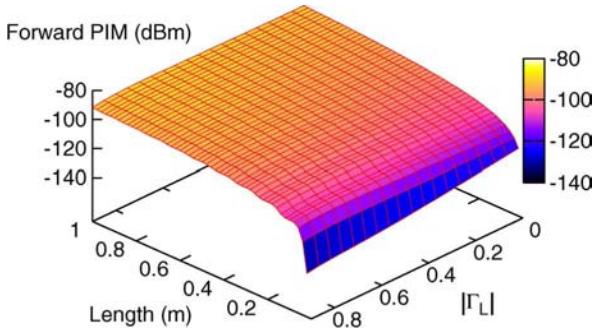

Fig. 8. Forward PIM3 on the microstrip lines with distributed nonlinearity terminated in the load with reflection coefficient $|\Gamma_L|$ at variable line length.

this phenomenon can be attributed to the effect of the carriers' standing waves in the line.

Indeed, in accordance with (2) and (3), the PIM3 level should grow as the third power of the carrier magnitude. Therefore, the standing waves of the carriers caused by the reflection from the load boost the process of the nonlinear conversion. As we can see in Fig. 6, at low $|\Gamma_L(\omega_{2,-1})|$, the latter effect exceeds return loss of forward PIM3 products due to reflection from the load. In other words, the nonuniform current distribution of carriers generates PIM3 harmonics with the higher rate than the reflection loss. However, at larger $|\Gamma_L(\omega_{2,-1})|$, this is no longer the case, and forward PIM3 level rapidly decays as $|\Gamma_L(\omega_{2,-1})|$ approaches the total reflection limit. The effect of $\Gamma_L(\omega_{2,-1})$ phase variations on the forward PIM3 generation is negligible, similar to the case of the reverse PIM products.

B. *Effect of the Line Length on PIM Generation*

The effect of the line length has already been discussed in Section V-A for the perfectly matched line. However, as demonstrated above, the load reflection had a strong impact on the PIM products, and therefore, the load mismatch should also affect PIM3 generation on the lines of different lengths.

To explore this effect, we have simulated PIM3 products generated on the microstrip lines of various lengths with the parameters of the experimental specimens used in Section III.

The simulation results are presented in Figs. 7 and 8. As seen in Fig. 7, the reverse PIM3 level does not grow fast with the line length at any $|\Gamma_L(\omega_{2,-1})|$. However, the surface of the reverse PIM3 products contains periodic troughs at low reflection. At higher $|\Gamma_L(\omega_{2,-1})|$, the surface topography becomes smoother as the PIM3 magnitude slowly increases. The most pronounced increase of the reverse PIM3 level occurs at short line length and high reflection.

In contrast to the reverse PIM3, the forward PIM3 level grows nearly monotonically with the line length at low reflection (cf. Fig. 8), but at large $|\Gamma_L(\omega_{2,-1})|$, small ripples appear on the surface. On the short lines, the forward PIM3 level grows fast similarly to the reverse PIM3 products, but the increment decreases on the longer lines and the forward PIM3 level starts to drop at higher $|\Gamma_L(\omega_{2,-1})|$.

These observations clearly indicate that losses and the distributed nonlinear scattering are the competing mechanism of PIM3 generation in printed lines. Harmonic generation dominates on short lines, and we witness substantial increase of PIM3 products. When the lines become longer, the two processes reach the equilibrium and the growth of PIM3 level becomes moderate. The load reflection in its turn plays a role of the third process. Namely, the reflection is responsible for the standing wave of carriers in the line that increases the magnitude of carriers engaged in the nonlinear process of harmonic generation. This explains significant increase in reverse PIM3 products and nonmonotonic dependence of the forward PIM3 products on $|\Gamma_L(\omega_{2,-1})|$.

VI. Conclusions

A comprehensive study of the mechanisms of PIM generation on printed lines has been carried out with the aid of the newly developed theoretical model for a section of transmission line with distributed weakly nonlinear resistance. Validity of the model has been confirmed by the excellent agreement with the

results of the near-field probing of PIM3 product distributions on microstrip lines.

Three major competitive processes have been identified and explored as the principal contributors to the PIM generation on printed lines: distributed nonlinear scattering, attenuation, and mismatch at the line terminations. It was shown that, in a lossless perfectly matched line, where the distributed nonlinear scattering was the only source of PIM3 products, the forward PIM level monotonically increases and exhibits the cumulative effect. The reverse PIM3 level shows regular variation with the line length, which suggests a means of reducing the PIM3 level by choosing the specific line lengths. It was demonstrated for the first time that the reverse PIM products are generated on the matched lines without carriers' reflection.

Losses in the line damp PIM products viz. reduce variations of the reverse PIM3 products and cap the growth of the forward PIM3 level with the line length. The forward PIM3 magnitude increases in the lines shorter than l_f, but decreases on the longer lines and even falls below the reverse PIM level as the line length exceeds the value of l_i defined by (23).

Reflection from the mismatched load creates the standing wave pattern of the carriers that causes nonuniform generation of PIM products along the line. On one hand, the reverse PIM level is increased owing to additional power engaged in the nonlinear scattering, particularly in the reverse propagating waves. On the other hand, the forward PIM products are reduced due to higher reflection from the load so that they may become comparable with the reverse PIM products even on the rather short lines.

APPENDIX

The particular inhomogeneous solution of (6) for the intermodulation harmonic at frequency $\omega_{2,-1}$ reads

$$\begin{aligned} F_{2,-1,1}(x) &= 3(i\omega_{2,-1}C+G) \\ &\times\left(\frac{A_{1,0,0}^2 A_{0,-1,0}\exp\left(-(2\gamma_{1,0}+\gamma_{0,-1})x\right)}{(2\gamma_{1,0}+\gamma_{0,-1})^2-\gamma_{2,-1}^2}\right. \\ &+\frac{A_{1,0,0}^2 B_{0,-1,0}\exp\left(-(2\gamma_{1,0}-\gamma_{0,-1})x-\gamma_{0,-1}l\right)}{(2\gamma_{1,0}-\gamma_{0,-1})^2-\gamma_{2,-1}^2} \\ &+\frac{2A_{1,0,0}B_{1,0,0}A_{0,-1,0}\exp(-\gamma_{0,-1}x-\gamma_{1,0}l)}{\gamma_{0,-1}^2-\gamma_{2,-1}^2} \\ &+\frac{2A_{1,0,0}B_{1,0,0}B_{0,-1,0}\exp\left(\gamma_{0,-1}(x-l)-\gamma_{1,0}l\right)}{\gamma_{0,-1}^2-\gamma_{2,-1}^2} \\ &+\frac{B_{1,0,0}^2 A_{0,-1,0}\exp\left((2\gamma_{1,0}-\gamma_{0,-1})x-2\gamma_{1,0}l\right)}{(2\gamma_{1,0}-\gamma_{0,-1})^2-\gamma_{2,-1}^2} \\ &\left.+\frac{B_{1,0,0}^2 B_{0,-1,0}\exp\left((2\gamma_{1,0}+\gamma_{0,-1})(x-l)\right)}{(2\gamma_{1,0}+\gamma_{0,-1})^2-\gamma_{2,-1}^2}\right). \quad \text{(A1)} \end{aligned}$$

ACKNOWLEDGMENT

The authors are grateful to Dr. O. Malyuskin and Dr. D. Linton, both with Queen's University of Belfast, Belfast, U.K., for the stimulating discussions. The authors also appreciate the generous support of Taconic Advanced Dielectric Division Ltd., Mullingar, Ireland, and Trackwise Designs Ltd., Tewkesbury, U.K.

REFERENCES

[1] M. T. Abuelma'atti, "Prediction of passive intermodulation arising from corrosion," *Proc. Inst. Elect. Eng.—Sci., Meas., Technol.*, vol. 150, no. 1, pp. 30–34, Jan. 2003.

[2] W. D. Watson, "The measurement, detection, location and suppression of external non-linearities which affect radio systems," in *Proc. Electromagn. Compat. Conf.*, Southampton, U.K., Sep. 1980, pp. 1–10.

[3] J. E. Erickson, "Intermodulation reduction in VHF communications systems," Griffiss Air Force Base, New York, NY, Rep. AD-AO17 486, Sep. 1975.

[4] C. Vicente, D. Wolk, H. L. Hartnagel, B. Gimeno, V. E. Boria, and D. Raboso, "Experimental analysis of passive intermodulation at waveguide flange bolted connections," *IEEE Trans. Microw Theory Tech.*, vol. 55, no. 5, pp. 1018–1028, May 2007.

[5] G. Macchiarella, G. B. Stracca, and L. Miglioli, "Experimental study of passive intermodulation in coaxial cavities for cellular base stations duplexers," in *Proc. 34th Eur. Microw. Conf.*, Amsterdam, The Netherlands, Oct. 2004, pp. 981–984.

[6] K. G. Gard, M. B. Steer, and J. R. Wilkerson, "Electro-thermal passive intermodulation distortion in microwave attenuators," in *Proc. 36th Eur. Microw. Conf.*, Manchester, U.K., Sep. 2006, pp. 157–160.

[7] A. K. Brown, "Passive intermodulation products in antennas-an overview," in *Proc. IEE Passive Intermod. Products in Antennas and Relat. Structures Colloq.*, London, U.K., Jun. 1989, pp. 1/1–1/3.

[8] A. P. Foord and A. D. Rawlins, "A study of passive intermodulation interference in space RF hardware," Univ. Kent, Canterbury, U.K., ESTEC Tech. Rep. 111036, May 1992, .

[9] J. Russer, A. Ramachandran, A. Cangellaris, and P. Russer, "Phenomenological modeling of passive intermodulation (PIM) due to electron tunneling at metallic contacts," in *IEEE MTT-S Int. Microw. Symp. Dig.*, San Francisco, CA, Jun. 2006, pp. 1129–1132.

[10] Z. Shi-quan and G. De-biao, "The generation mechanism and analysis of passive intermodulation in metallic contacts," in *Proc. 4th Asia–Pacific Environ. Electromagn. Conf.*, Dalian, China, Aug. 2006, pp. 546–549.

[11] A. G. Schuchinsky, J. Francey, and V. F. Fusco, "Distributed sources of passive intermodulation on printed lines," in *Proc. IEEE AP-S Int. Symp.*, Washington, DC, Jul. 2005, pp. 447–450.

[12] S. Hienonen and A. V. Räisänen, "Passive intermodulation near-field measurements on microstrip lines," in *Proc. 34th Eur. Microw. Conf.*, Amsterdam, The Netherlands, Oct. 2004, pp. 1041–1044.

[13] S. Hienonen, V. Golikov, P. Vainikainen, and A. V. Räisänen, "Near-field scanner for the detection of passive intermodulation sources in base station antennas," *IEEE Trans. Electromagn. Compat.*, vol. 46, no. 4, pp. 661–667, Nov. 2004.

[14] N. Kuga and T. Takao, "Passive intermodulation evaluation of printed circuit board by using 50 Ω microstrip line," in *Proc. Asia–Pacific Microw. Conf.*, New Delhi, India, Dec. 2004, pp. 1008–1009.

[15] J. V. S. Pérez, F. G. Romero, D. Rönnow, A. Söderbärg, and T. Olsson, "A microstrip passive intermodulation test set-up; comparison of leaded and lead-free solders and conductor finishing," in *Proc. Int. Multipactor, Corona, Passive Intermod. Workshop*, Noordwijk, The Netherlands, Sep. 2005, pp. 215–222.

[16] J. A. Jargon, D. C. DeGroot, and K. L. Reed, "NIST passive intermodulation measurement comparison for wireless base station equipment," in *Proc. 52nd ARFTG Comput.-Aided Design and Test for High-Speed Electron. Conf.*, Rohnert Park, CA, Dec. 1998, pp. 128–139.

[17] S. Hienonen and A. V. Räisänen, "Effect of load impedance on passive intermodulation measurements," *Electron. Lett.*, vol. 40, no. 4, pp. 245–247, Feb. 2004.

[18] S. Hienonen, "Studies on microwave antennas: Passive intermodulation distortion in antenna structures and design of microstrip antenna elements," Doctor Sci. Technol. dissertation, Helsinki Univ. Technol., Espoo, Finland, 2005.

[19] D. E. Zelenchuk, A. P. Shitvov, A. G. Schuchinsky, and T. Olsson, "Passive intermodulation on microstrip lines," in *Proc. 37th Eur. Microw. Conf.*, Munich, Germany, Oct. 2007, pp. 396–399.

[20] D. E. Zelenchuk, A. P. Shitvov, and A. G. Schuchinsky, "Effect of matching on passive intermodulation in transmission lines with distributed nonlinear resistance," presented at the Int. URSI Commission B–Electromagn. Theory Symp., Ottawa, ON, Canada, Jul. 2007, Art. ID R19-39, EMTS171.

[21] A. P. Shitvov, D. E. Zelenchuk, A. G. Schuchinsky, V. F. Fusco, and N. Buchanan, "Mapping of passive intermodulation products on microstrip lines," in *IEEE MTT-S Int. Microw. Symp. Dig.*, Atlanta, GA, Jun. 2008, Paper THP2H-02.
[22] A. P. Shitvov, D. E. Zelenchuk, and A. G. Schuchinsky, "Experimental observations of distributed nonlinearity in printed transmission lines," in *Proc. 14th Int Microw. Opt. Appl. Novel Phys. Phenomena. Student Seminar*, Belfast, U.K., Aug. 2007, pp. 70–72.
[23] R. E. Collin, *Foundation for Microwave Engineering*, 2nd ed. New York: McGraw-Hill, 1992.
[24] B. A. Auld, M. Didomenico, Jr., and R. H. Pantell, "Traveling-wave harmonic generation along nonlinear transmission lines," *J. Appl. Phys.*, vol. 33, pp. 3537–3545, Dec. 1962.
[25] K. Itô, *Encyclopedic Dictionary of Mathematics*, 2nd ed. Cambridge, MA: MIT Press, 1993, ch. 269A, p. 994.
[26] A. P. Shitvov, D. E. Zelenchuk, and A. G. Schuchinsky, "Distributed model of passive intermodulation phenomena in printed transmission lines," in *Proc. Int. Microw. Appl. Novel Phys. Phenomena Student Seminar*, Rovaniemi, Finland, Aug. 2006, pp. 61–63.
[27] M. A. R. Gunston, *Microwave Transmission—Line Impedance Data*. New York: Van Nostrand, 1972.
[28] J. A. Armstrong, N. Bloembergen, J. Ducuing, and P. S. Pershan, "Interactions between light waves in a nonlinear dielectric," *Phys. Rev.*, vol. 127, no. 6, pp. 1918–1939, Sept. 1962.
[29] F. Abbas, "Measurements of passive intermodulation in 2G and 3G," in *Proc. 32nd Eur. Microw. Conf.*, Milan, Italy, Oct. 2002, pp. 1–4.

Dmitry E. Zelenchuk (S'02–M'05) received the B.Sc. and M.Sc. degrees in physics and Ph.D. degree in radiophysics from Rostov State University, Rostov-on-Don, Russia, in 1999, 2001, and 2004, respectively.

From 2003 to 2005, he was a Lecturer with the Department of Applied Electrodynamics and Computer Modelling, Rostov State University. He is currently a Research Fellow with Queen's University Belfast, Belfast, U.K. He has authored or coauthored over 40 journal and conference papers. His research interests include numerical and analytical methods for the problems of electromagnetic field theory, numerical modeling of frequency-selective surfaces, linear and nonlinear phenomena in planar circuits and antennas including PIM, and various physical phenomena of plasmonic and nanostructures.

Dr. Zelenchuk was the recipient of the Medal of the Ministry of Education of the Russian Federation for the Best Scientific Student Paper in 2001.

Aleksey P. Shitvov received the Diploma Specialist degree in semiconductor devices and microelectronics from Nizhny Novgorod State University (NNSU), Nizhny Novgorod, Russia, in 1995, and is currently working toward the Ph.D. degree at Queen's University of Belfast, Belfast, U.K.

From 2000 to 2004, he was a Research Assistant with the Department of Electronics, NNSU, where he was involved with the design and simulation of devices based on surface acoustic waves. His current research is focused on PIM phenomena in printed lines and PCB laminates. His research interests include experimental design and measurements of PIM products on PCBs and phenomenology of nonlinear responses of printed lines.

Alexander G. Schuchinsky (M'97–SM'05) received the M.Sc. degree in radiophysics from Rostov State University, Rostov-on-Don, Russia, in 1973, and the Ph.D. degree in radiophysics from the Leningrad Electrotechnical Institute, Leningrad, Russia, in 1983, respectively.

In 1988, he was awarded the academic title of Senior Research Scientist. From 1973 to 1994, he was with the Microwave Electrodynamics Laboratory, Rostov State University, where he held was a Leading Scientist. From 1994 to 2002, he was with Deltec-Telesystems New Zealand. Since 2002, he has been a Reader with the School of Electronics, Electrical Engineering and Computer Science, Queen's University Belfast, Belfast, U.K. He has authored or coauthored over 130 papers in major journal and conference proceedings. He holds three U.S. patents. He is a member of the Editorial Board of *Metamaterials*. His current research interests include numerical–analytical and physics-based modeling techniques, microwave and optical phenomena in complex media, metamaterials, periodic structures with linear and nonlinear inclusions, electromagnetic characterization and measurements of materials, and microwave applications of novel materials.

Dr. Schuchinsky is a member of the European Physical Society. He serves as a chair of the Steering Committee of the International Congress on Advanced Electromagnetic Materials in Microwaves and Optics (Metamaterials'2007).

Vincent F. Fusco (S'82–M'82–SM'96–F'04) received the Bachelors degree in electrical and electronic engineering (first-class honours), Ph.D. degree in microwave electronics, and D.Sc. degree (for his work on advanced front-end architectures with enhanced functionality) from the Queen's University of Belfast, Belfast, U.K., in 1979, 1982, and 2000, respectively.

Since 1995, he has held a personal chair in High Frequency Electronic Engineering with the Queen's University of Belfast. He is currently Research Director of the High Frequency Laboratories, Electronics, Communications and Information Technologies (ECIT), Queen's University of Belfast, and is Director of the International Centre for Research for System on Chip and Advanced Microwireless Integration (SoCaM). He has authored or coauthored 350 scientific papers in major journals and referred international conferences, and has authored two text books. He holds several patents and has contributed invited chapters to books in the field of active antenna design and electromagnetic (EM) field computation. His research interests include nonlinear microwave circuit design and active and passive antenna techniques. The main focus for this research is in the area of wireless communications. He has pioneered many new concepts in self-tracking antenna technology.

Prof. Fusco is a Fellow of the Royal Academy of Engineering and the IEE. He was the recipient of a 1986 British Telecommunications Fellowship and a 1997 Northern Ireland Engineering Federation Trophy for outstanding industrially relevant research.